RSC Advances

Solvent-induced self-assembly synthesis of ultralong single crystalline organic NiOEP nanowires with high photoconductivity

Journal:	*RSC Advances*
Manuscript ID:	RA-ART-07-2015-014266.R1
Article Type:	Paper
Date Submitted by the Author:	13-Aug-2015

Complete List of Authors:	Wang, Juan-Ye; Suzhou Institute of Nano-tech and Nano-bionics, Chinese Academy of Sciences, Peng, hongdan; Suzhou Institute of Nano-tech and Nano-bionics, Chinese Academy of Sciences, Yang, Jia-Mei; Suzhou Institute of Nano-tech and Nano-bionics, Chinese Academy of Sciences, Yan, Jinghui; Changchun University of Science and Technology, School of Chemical and Environmental Engineering Pan, Ge-Bo; Suzhou Institute of Nano-tech and Nano-bionics, Chinese Academy of Sciences,

Journal Name

ARTICLE

Solvent-induced self-assembly synthesis of ultralong single crystalline organic NiOEP nanowires with high photoconductivity

Received 00th January 20xx,
Accepted 00th January 20xx

DOI: 10.1039/x0xx00000x

www.rsc.org/

Juan-Ye Wang,[ab] Hong-Dan Peng,[b] Jia-Mei Yang,[b] Jing-Hui Yan*[a] and Ge-Bo Pan*[b]

We develop a facile approach for the one-step growth of ultralong and high-quality NiOEP nanowire in a large area, through solvent-induced self-assembly method without using any structure directing agent. The size of the nanowires can be controlled by changing the composites of solvent mixtures. Being assembled in visible-light sensors, these nanowires exhibit a fast, reversible, and stable response. The highest I_{on}/I_{off} ratio and photoresponsivity of photodiodes could reach 681 and 10.1 mA W^{-1}, respectively, which could be attributed to the perfect single-crystal quality, large surface to volume ratio, and fewer recombination barriers within the nanostructures. The facile fabrication and good photoresponse make NiOEP nanowires promising in optoelectronic applications.

Introduction

Single crystalline, one-dimensional (1D) nanostructures of organic semiconductors have recently attracted a surge of interest because of their promising applications in high performance optical and electronic devices like photodetectors.[1-4] Importantly, compared to their inorganic counterparts, organic semiconducting nanowires provide great inherent advantages including solution processability, simplicity of designing molecules to tune electronic properties, and ease of large area fabrication.[5] So far, various synthetic methods have been developed to fabricate organic nanowires, for example, electrospining,[5] physical vapor deposition (PVD),[6] solvent-vapor annealing,[7] and self-assembly approach from solution.[8] Among them, the latter technique as an efficient and versatile bottom-up method is of particular interest because the simplicity of fabrication implies minimized processing costs.

Porphyrin and its derivatives are one of superstar organic semiconductor materials that offer a variety of unique optical, electrochemical, field emission, and catalytic properties, which are dependent on center metals and different peripheral substituents.[9,10] Single-crystalline porphyrin nanowires with large length/diameter aspect ratio can be expected to facilitate superior device performance due to enhanced π-π conjugated morphology and the establishment of charge transport according to the molecular packing orientation. Thus, it is highly desirable to explore a feasible method for ultralong porphyrin nanowires. However, the control over the organization and morphology of porphyrin assemblies with a desirable size, shape and therefore function remains challenging. To date, there are relatively few reports on 1D porphyrin nanostructures-based nanodevices aimed various applications.[11-17]

The assembled morphologies are not only mainly dependent on the composition and structure of organic molecules, but also they are influenced by the self-assembly method and the outer environment including the kinds of solvents, solution concentration, and the composition of solvent mixture. The strong π-π interaction between the planar aromatic skeleton and non-collapsible structure makes NiOEP ideal candidate for 1D self-assembly. However, according to the previous reports, the average length of the obtained NiOEP micro/nanowires with the low aspect ratio was limited to only several or tens micrometers,[11,18,19] resulting in the difficulty of the nanoscaled device fabrication.

In our previous work, the non-volatile and viscous ionic liquids or high boiling solvent propylene glycol methyl ether acetate (PGMEA) was used to prepare zinc octaethylporphyrin nanowires (ZnOEP) nanowires. However, these methods inevitably induced the tedious and time-consuming solvent post-treatment. As part of our continuous efforts toward the fabrication of ordered porphyrin nanostructures,[20,21] here we report the fabrication and optoelectronic properties of ultralong NiOEP nanowires. It is found that the ultralong, highly uniform, and single crystalline NiOEP nanowires with smooth surface can be obtained conveniently by the mixed solvent techniques[22, 23] at ambient conditions without surfactant or additional templates. The prototype photodetectors based on these nanowires show fast, reversible, and stable response with switch ratio over 600.

Experimental

[a] College of Chemistry and Environmental Engineering, Changchun University ofScience and Technology, 130022 Changchun, China. E-mail: yjh@cust.edu.cn.
[b] Suzhou Institute of Nano-tech and Nano-bionics, Chinese Academy of Sciences,215123 Suzhou, P. R. China. E-mail: gbpan2008@sinano.ac.cn;Fax: +86-512-62872663.

† Electronic supplementary information (ESI) available: Optical images, molecule stacking; energy band; geometry of finger electrode.
See DOI: 10.1039/x0xx00000x

Fabrication: NiOEP was purchased from Sigma-Aldrich and used without further purification. The solvents of chloroform and ethyl acetate (EtOAc) were purchased from the Aladdin Company. The nanowires were prepared by solution process. NiOEP powder was dissolved into chloroform followed by ultrasonication for 30 min. The final solution was than rapidly injected into EtOAc. Finally, a drop (~25 μl) of the mixed solution is deposited onto a (5 mm × 5 mm) heavily doped n-type Si substrate covered with 300 nm thick SiO_2. To remove the solvent thoroughly, the obtained nanowires were post-annealed at 150 ^oC for 1 h.

Characterization: The products were characterized by the X-ray diffraction pattern (XRD) obtained using a Bruker D8 Advance powder X-ray diffractometer. The morphology and structure were examined on a Hitachi-S4800 scanning electron microscope (SEM) and a Tecnai G2 F20 S-Twin transmission electron microscope (TEM). The selected area electron diffraction (SAED) pattern was taken simultaneously on a Tecnai G2 F20 S-TEM. Energy-dispersive X-ray spectrometry (EDX) analysis was performed on the Quanta 400 FEG SEM. Diffuse reflectance UV-vis absorption spectra were recorded on a Perkin-Elmer Lambda 750 equipped with a 60 mm integrating sphere. Fourier transform infrared (FTIR) spectra were acquired using a Nicolet 760 FTIR spectrometer in a KBr pellet.

Device fabrication and measurement: The photodetector device structure was constructed in a bottom-connected configuration. The finger electrodes with the length of 200 μm, the width of 20 μm, and the distance of 20 μm were fabricated by the photolithography and electron beam deposition of Au on SiO_2/Si. The chloroform solution of NiOEP at a concentration of about 3.6 mg ml^{-1} was rapidly injected into EtOAc. The volume ratio of chloroform and EtOAc was 1:2. A drop of NiOEP solution is deposited on the Au electrodes and the solvent is allowed to evaporate in air. To remove the solvent thoroughly, the device is post-annealed at 150^oC for 1 h. Current-voltage characteristics of the devices were recorded with Keithley 4200 SCS and SUSS PM8 probe station in a clean and shielded box at room temperature. A Xenon lamp was used as the white light source with different intensity.

Results and discussion

Fig. 1a shows a representative scanning electron microscopy(SEM) image of the as-obtained sample. The volume ratio of chloroform and EtOAc was 1:2, and the concentration of mixed solution was 1.2 mg ml^{-1}.It can be seen that ultralong nanowires with smooth surfaces have been formed. The nanowires have average diameters ranging from 300 to 600 nm, and average lengths up to 700 μm. The optical image and distribution of length are shown in Fig.S1†. Fig. 1b shows a typical transmission electron microscopy (TEM) image of a single nanowire, indicating that it is solid and has a uniform diameter. The chemical composition of nanowires is analyzed by energy dispersive X-ray spectroscopy (EDX). The EDX spectrum clearly indicates the existence of Ni element in Fig.1c. The crystalline structure of NiOEP nanowires is investigated by X-ray diffraction (XRD) and selected area electron diffraction (SAED) (Fig. 1d). The diffraction peaks in the XRD pattern of NiOEP nanowires can be indexed to a triclinic phase. The lattice constants are a= 13.302 Å, b = 13.342 Å, c = 4.802 Å, α =92.21 °, β = 91.177 °, and γ = 92.157 °.[18,23] Moreover, the diffraction peak of $(11^{-1}0)$ planes of the nanowires corresponding to the 2θ value of 7.96° is significantly sharp, revealing a highly crystalline feature of these nanowires. This was possibly attributed to the preferential growth of high-aspect-ratio nanowires, which are driven by strong molecular stacking between NiOEP skeletons. This was further confirmed by the well-defined SAED pattern of a single NiOEP nanowire. The growth direction of NiOEP nanowires is along the (001) direction, i.e., the self-assembly direction of NiOEP molecule stacking by intermolecular π-π interactions. The stacking direction of NiOEP molecules is shown in Fig.S2†and the intermolecular π-π distance is about 3.472Å.[18]

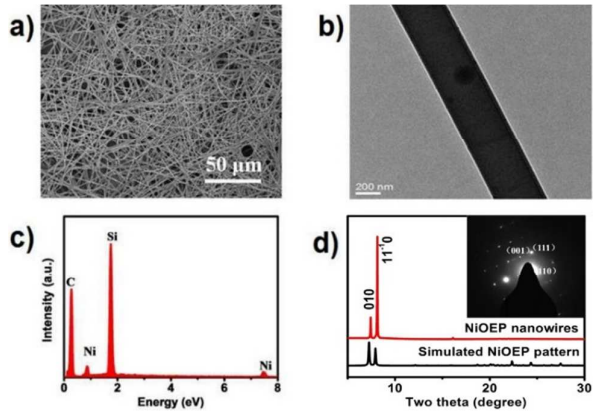

Fig. 1(a) SEM and (b) TEM images of NiOEP nanowires. (c) EDX and (d) XRD patternof NiOEP nanowires (red) and simulated pattern from the single crystal data (CCDC, Refcode: NOEPPR02).The inset was an SAED pattern recorded for a single NiOEP nanowire.

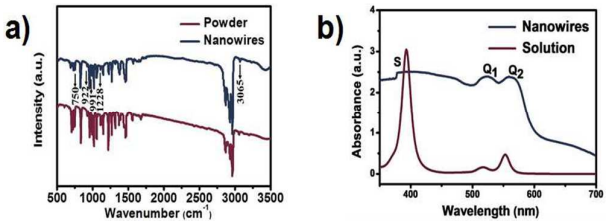

Fig. 2 (a) FTIR and (b) UV-vis absorption spectra of nanowires and source powder of NiOEP.

Fourier-transform Infrared (FTIR) spectra, as shown in Fig. 2a, were measured to analyze the chemical composition of these nanowires and possible structure change after fabrication. It is clear that the FT-IR spectrum of nanowires has the same feature as that of the source powder of NiOEP. Four metal-sensitive IR characteristic bands of octaethylporphyrin are observed at 750, 922, 991, and 1228 cm^{-1}, implying that NiOEP does not undergo decomposition or other chemical reactions. Fig. 2b shows typical UV-vis absorption spectra of nanowires deposited on quartz and NiOEP monomers in chloroform solution. NiOEP monomers display an extremely intense band, the so-called Soret or B-bands in the 380-430 nm, corresponding to the transition from the ground state to the second excited state ($S_0 \rightarrow S_2$). At longer wavelengths, in the 500-600 nm range, their spectra contained two weaker, but still considerably

intense Q bands, consisting of a weak transition to the first excited state ($S_0 \rightarrow S_1$).Similar to the monomers, the nanowires have three characteristic adsorption bands, labeled as S, Q_1, and Q_2. It is noted that the bands of nanowires are broadened in comparison with the sharp peaks from the monomers. Moreover, the Q bands are red-shifted, whereas the S band is blue-shifted. This can be attributed to the highly ordered molecule-packing in NiOEP nanowires. Thus, their absorption bands of NiOEP nanowires significantly overlap with visible-light region.

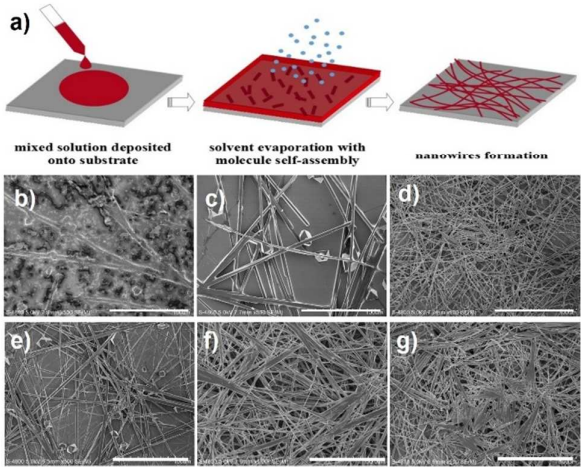

Fig. 3 (a) Schematic illustration of the fabrication process of the NiOEP nanowires. SEM images of NiOEP nanostructures fabricated at 1.2 mg ml^{-1} with different volume ratios of chloroform and EtOAC ($V_{chloroform}/V_{EtOAC}$): (b) 1:0; (c) 3:1; (d) 1:3; SEM images of NiOEP nanostructures fabricated at volume ratios of chloroform and EtOAC 1:3 with different concentrations: (e) 0.8 mg/ml; (f) 1.4 mg/ml; and (g) 1.6 mg/ml. Scale bar: 100 μm.

Fig.3 (a) shows the fabrication process of NiOEP nanowires by utilizing self-assembly at solution-substrate interface upon solution evaporation. To understand the morphological evolution of the nanowires, the influences of different the volume ratio of chloroform and EtOAc and the concentration of mixed solution were investigated. When approximately 10μL of 1.2 mg/mL chloroform solution was drop-cast on silicon substrate at room temperature, aggregated particles were formed, which is probably due to low boiling point and rapid evaporation of chloroform (Fig3b). To reduce the evaporation speed and elongate the self-assembly of NiOEP, we prepared $CHCl_3$-EtOAc (v/v, 3:1) solution with the same concentration. As expected, microwires with the length of ~200 to 300 μm and the width of ~2 to 3μm were obtained after solution evaporation (Fig.3c). Interesting, very small octahedral nanostructrues were also observed. However, further increase the EtOAC volume content of the mixed solvent to 75%, it can be observed that the products have high morphological purity, very uniform diameter and smooth surface through their entire length (Fig.3d). These results indicate that a simple reduction in the evaporation speed has a large influence on the self-assembly kinetics of NiOEP in solution and leads to a drastic change in the geometry of the resultant structures.

Since the self-assembly of different concentration solutions is the same environment, if we ignore the effect of concentration to the evaporation of solvent, we can assume the evaporating rates of the solutions (with different concentrations) are same. Thus, when different concentrations of solutions (10μL) at the fixed volume ratio of $CHCl_3$-EtOAc (3:1) were drop cast to the silicon substrate, higher initial concentration solution reaches supersaturation faster than the lower one. As shown in Fig. 3e, when the concentration was as low as 0.8mg/mL, the separated microwires mixed with octahedral nanoparticles were obtained. Increasing the NiOEP concentration promoted the formation of pure nanowires network with longer length and smaller diameter as a result of the adequate for the continuous growth (Fig. 3f). However, when the concentration is up to 1.6mg/mL, the evaporation of the solution caused the high growth speed of crystal and produced a large number of nucleation points, thus the nanowires tended to aggregate and their distribution became less uniform (Fig. 3g).

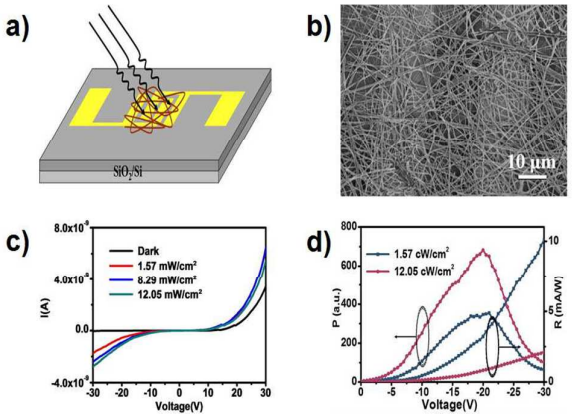

Fig. 4 (a) Schematic illustration and (b) SEM image of prototype device of NiOEP nanowires. (c) Dark current and photocurrent at different incident power densities. (d) Photoresponsivity (R) and photocurrent/dark current ratio (P) versus V bias under illumination with 1.57 mW cm^{-2} and12.05 mW cm^{-2}.

To explore its photoresponse characteristics, a prototype device is constructed. Fig. 4a is a schematic illustration of a nanowires-based device. Fig. 4b shows a typical SEM image of the as-constructed device. It is clear that the nanowires have been connected to two Au electrodes. Fig. 4c shows the typical I-V curves of the device in the dark and under continuous white light illumination. At low voltage section, the photocurrent without significant increase indicates that there is Schottky energy barrier at the contact between the nanowires and Au electrode (Fig. S3†).[25] As the voltage further increases, the photocurrent under light illumination is markedly higher than that obtained in the dark. At an applied bias of -20 V, the NiOEP nanowires in the dark show a relatively low current of 1.58pA. At a low power density of1.57 mW cm^{-2}, an electrical current of 547.2 pA is obtained. This corresponds to a photocurrent on/off ratio of ca. 346. The I_{light}/I_{dark} ratio is expected to be much larger if higher power illumination and/or longer electrode pairs are

employed for the photocurrent measurement. At a high power density of 8.29 mW cm^{-2}, the photocurrent on/off ratio reaches 583.

Photosensitivity (I_{light}/I_{dark} ratio, P) and photoresponsivity(R) are two important parameters for photodetectors.[26, 27]As shown in Fig. 4d, P varies with the applied voltage and light intensity. The P_{max} can reach 681 with the intensity of 12.05 mW cm^{-2} at -20 V. The R can be defined as R=I/PS,[27] where I is the photocurrent, P is the incident light intensity, and S is irradiated area. It is noted that the real area of nanowire network film is generally difficult to be defined. This is mainly because the coverage and specific surface area of nanowires can't be controlled exactly. Therefore, the effective area, estimated from the equation of 3×L×W, is used to calculate the responsivity of R for simplicity. Similar to thin films, W and L are the width and length of channel, respectively. (Fig. S5†) The value is much higher than that of CoOEP naonwires.[28] In addition, it is seen that R is also dependent on the voltage except the light intensity, which increases with increasing the applied voltage, indicating some field-assisted exciton dissociation close to the interface. The calculated maximum of R reaches 10.1 mA W^{-1} at -30 V under an illumination intensity of 1.57 mW cm^{-2}.

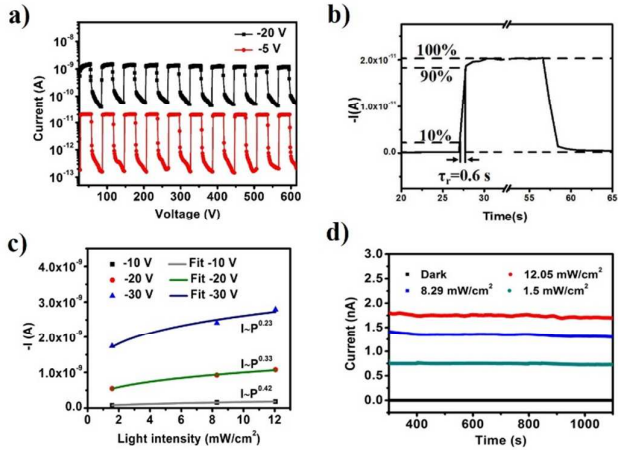

Fig.5 (a) Time-dependent on/off switching of the device based on NiOEP nanowires. (b) The response time (τr) of the device based on NiOEP nanowires. (c) Photocurrent versus incident optical densities measured at bias voltages of -10 V, -20 V and -30 V. (d) Current versus time continuously over 800 s in the dark and under illumination.

On the basis of the active photosensitivity, the time-dependent photoresponse of the device is measured by periodically turning the white light on and off. Fig. 5a shows the typical on/off characteristic with the light turning on and off. The light power is 12.05mW cm^{-2} and the applied voltage is -5V and -20V, respectively. It is clear that the current of the devices shows two distinct states, a "low" current state in the dark and a "high" current state under illumination. The "on"- and "off"-state currents for 8 cycles remain almost the same. Fig. 5b gives the enlarged view of a single on/off cycle of the flexible device in which the 10% and 90% points to the peak value of the photocurrent are ticked for calculating the response time. From the curve, it can be seen that the typical response time is ca. 0.6 s from the "off"- to "on"-state, which is shorter than that of the ZnOEP nanowires reported in the literature.[20] The above values indicate reversible, fast, and stable photoswitch characteristics. Fig. 5c shows the relationship between photocurrent and incident light power density. The fitting demonstrates a power dependence of ~0.42 at -10 V, ~0.33 at -20 V, and ~0.23 at -30 V. The non-unity exponent was a result of the complex process of electron-hole generation, trapping, and recombination within the semiconductor.[29] As shown in Fig. 5d, the current in the dark remains almost constant, while the photocurrent at -30 V with an illumination intensity of 12.05 mW cm^{-2} nearly holds steady. After 800s, the photocurrent only decreases by 1.6% at 1.57 $mWcm^{-2}$, 4.1 % at 8.29 $mWcm^{-2}$, 2.8 % at 12.05 $mWcm^{-2}$, respectively. This phenomenon might be attributed to the change of electric contact and the influence of the surface state (including surface defects and oxygen adsorption/desorption process). The above results suggest the potential application of NiOEP nanowires-based devices for the high-sensitivity and high-stability nanoscale photodetectors and photoelectrical switches.

Conclusions

In summayr, we report a facile and scalable synthesis of ultralong and high-quality NiOEP nanowires via solvent-induced self-assembly method without using any structure directing agent and their photoconductive characteristics were first fully investigated. The as-obtained NiOEP nanowires are single-crystals grown along the (001) direction with a uniform diameter of 300-600 nm and a typical length of hundreds of micrometers. Being assembled in visible-light sensors, these nanowires exhibit a fast, reversible, and stable response. The highest I_{on}/I_{off} ratio and photoresponsivity of photodiodes could reach 681 and 10.1 mA W^{-1}, respectively, which could be attributed to the perfect single-crystal quality, large surface to volume ratio, and fewer recombination barriers within the nanostructures. These results suggest that NiOEP nanowires obtained by this strategy have great potential as promising blocks for future high sensitivity and high stability photodetectors.

Acknowledgements

The authors gratefully acknowledge the financial support from the National Natural Science Foundation of China (21273272), the China Postdoctoral Science Foundation (2013M541747), the Jiangsu Planned Projects for Postdoctoral Research Funds (1302159c), and the Chinese Academy of Sciences.

Notes and reference

1. S. Y. Min, T. S. Kim, Y. Lee, H. Cho, W. T. Xu and T. W. Lee, *Small*, 2015, 11, 45.
2. F. S. Kim, G. Q. Ren and S. A. Jenekhe, *Chem. Mater.*,2011, 23, 682.
3. Y. B. Guo, L. Xu, H. B. Liu, Y. J. Li, C. M. Che and Y. L. Li, *Adv. Mater.*,2015, 27, 985.
4. H. Yu, D. Y. Kim, K. J. Lee and J. H. Oh, *J. Nanosic.*

Nanotechnol., 2014, 14, 1282.
5. A. Greiner, J. H. Wendorff, *Angew. Chem. Int. Ed.*, 2007, 46, 5670.
6. Q. X. Tang, H. X. Li, M. He, W. P. Hu, C. M. Liu, K. Q. Chen, C. Wang, Y. Q. Liu and D. B. Zhu, *Adv. Mater.*, 2006, 18, 65.
7. A. Datar, R. Oitker, L. Zang, *Chem. Commun.*, 2006, 1649.
8. X. J. Zhang, J. S. Jie, W. F. Zhang, C. Y. Zhang, L. B. Luo, Z. B. He, X. H. Zhang, W. J. Zhang, C. S. Lee and S. T. Lee, *Adv. Mater*., 2008, 20, 2427.
9. C. J. Medforth, Z. C. Wang, K. E. Marin, Y. J. Song, J. L. Jacobsen and J. A. Shelnutt, *Chem. Commun.*, 2009, 7261.
10. C. M. Drain, A. Varotto and I. Radivojevic, *Chem. Rev.*, 2009, 109, 1630.
11. J. S. Hu, H. X. Ji, L. J. Wan, *J. Phys. Chem. C*, 2009, 113, 16259.
12. H. X. Ji, J. S. Hu, L. J. Wan, *Chem. Commun*., 2008, 2653.
13. J. H. Cai, H. H. Chen, J. Huang, J. X. Wang, D. L. Tian, H. Dong and L. Jiang, *Soft Mater.*, 2014, 10, 2612.
14. A. D. Schwab, D. E. Smith, B. Bond-Watts, D. E. Johnston, J. Hone, A. T. Johnson, J. C. de Paula and W. F. Smith, *Nano letters*, 2004, 4, 1261.
15. T. F. Liu, Y. J. Li, Y. Li, Y. L. Li, Y. W. Yu, N. Chen, S. H. Chen, C. Liu, Y. S. Zhao and H. B. Liu, *J. Phys. Chem. C*, 2012, 116, 14143.
16. E. M. Garcia-Frutos, *J. Mater. Chem. C*, 2013, 1, 3633.
17. S. Toksoz, H. Acar and M. O. Guler, *Soft Matter*, 2010, 5839.
18. M. H. So, V. A. L. Roy, Z. X. Xu, S. S. Y. Chui, M. Y. Yuen, C. M. Ho, and C. M. Che, *Chem. Asian J*., 2008, 3, 1968.
19. Z. X. Xu, H. F. Xiang, V. A. Roy, S. S. Chui, C. M. Chi and P. T. Lai, *Appl. Phys. Lett.*, 2006, 93, 223305.
20. F. X. Wang, J. Lin, W. B. Gu, Y. Q. Liu, H. D. Wu and G. B. Pan, *Chem. Commun*., 2013, 49, 2433.
21. Q. G. Zhang, Y. Lu, F. X. Wang, Y. Wei, Y. Q. Liu, B. Yang and G. B. Pan, *RSC Adv.*, 2014, 4, 47325.
22. X. C. Gong, T. Milic, C. Xu, J. D. Batteas and C. M. Drain, *J. Am. Chem. Soc.*, 2002, 124, 14290.
23. M. Zhao, S. Wang, Q. L. Bao, Y. Wang, P. K. Ang and K. P. Loh. *Chem. Commun*., 2011, 47, 4153.
24. 24 T. D. Brennan, W. R. Scheidt and J. A. Shelnutt, J. Am. Chem. Soc. , 1998, 110, 3919-3924.
25. L. Scudiero, D. E. Barlow, and K. W. Hipps, *J. Phys. Chem. B*, 2002, 10, 996.
26. H. Yu, Z. Bao and J. H. Oh, *Adv. Funct. Mater*., 2013, 23, 629.
27. M. C. Hamilton, S. Martin, J. Kanicki, *IEEE Trans. Electron. Device*, 2004, 51, 877.
28. F. X. Wang, Y. Q. Liu, H. D. Wu and G. B. Pan, *Mater. Res. Express*, 2014, 1, 016303.
29. N. Ai, Y. Zhou, Y. Zheng, H. B. Chen, J. Wang, J. Pei, Y. Cao, *Organic Electronics*, 2013, **14**, 1103-1108.